

Quantum reflection of atoms from a periodic dipole potential

N. Friedman, R. Ozeri, and N. Davidson

Department of Physics of Complex Systems, Weizmann Institute of Science, Rehovot 76100, Israel

Received November 14, 1997; revised manuscript received February 18, 1998

Quantum reflection of neutral atoms from a periodic far-detuned dipole potential is proposed and analyzed. This periodic atom mirror relies on constructive interference of small reflections from each cell to yield a high reflection coefficient even for very weak potentials. The reflected energy spectrum is calculated as a function of the potential height and the number of cells for both positive and negative potentials, and its relation to the reflection from one potential cell is derived. Two ways of increasing the reflection bandwidth, one based on changing the envelope of the potential and the other on changing its period gradually (chirp), are investigated. The phase of the reflected atoms and its dependence on experimental parameters are calculated, as well as the interaction time of the atoms with the potential and the spontaneous-emission rate during the reflection. Finally, it is shown that atoms with velocities of a few tens mm/s can be coherently reflected from a negative periodic potential with readily available laser diodes. © 1998 Optical Society of America

[S0740-3224(98)02705-2]

OCIS code: 140.3320.

1. INTRODUCTION

In the past few years, several experiments have demonstrated the reflection of atoms from laser light fields.¹⁻³ These atom mirrors consist of evanescent light that escapes from a dielectric medium, and the atoms are reflected from the dipole potential created by the light field. In these mirrors the kinetic energy of the atoms is lower than the maximal potential height, and the reflection can be understood from classical considerations. However, particles with kinetic energy that is higher than the potential can also be reflected, according to quantum mechanics. Recently, such quantum reflection of cold atoms from negative potential (red-detuned evanescent wave) was suggested.⁴ The reflection in that case is limited to very cold atoms, with kinetic energy lower than the atom's recoil energy $E_R = \hbar^2 k_L^2 / 2m$ (k_L is the laser wave number, and m is the mass of the atom). The limit on the reflected energy is due to the limited depth and the steepness of the potential that can be achieved. As an example, a laser with intensity of $\sim 10^4$ mW/cm², red detuned 100 GHz (0.2 nm) from the ⁸⁵Rb $5S_{1/2} \rightarrow 5P_{3/2}$ (D_2) transition, and a penetration depth of 200 nm of the evanescent wave into the vacuum will reflect atoms with velocity of only 0.4 mm/s (1/15 of the recoil velocity) with a probability of 50%.

As is known from optics, reflection can be enhanced by the use of periodic structures, in which small reflections from many interfaces interfere constructively, to form a high total reflection. The same idea can be used to reflect cold atoms from a periodic light structure (e.g., a standing wave) that induces a periodic potential $U(x) = U(x + \Lambda)$ through the light-atom dipole interaction. For certain energies the reflections from all the potential cells interfere constructively, and atoms at these energy bands are totally reflected. As we show below, such a periodic

potential can reflect atoms with much higher energy than in the nonperiodic case.

Interactions of atoms with periodic light structures were investigated extensively in past years, in various experiments in one-dimensional^{5,6} (1-D) and three-dimensional^{7,8} optical lattices. In particular, phenomena that reveal the long-range spatial order in the lattice, such as Bragg reflection of light from the bounded atoms, were demonstrated.^{9,10} In the case of 1-D lattices, analogy to solid state physics was demonstrated in phenomena like Bloch oscillations¹¹ and Wannier-Stark ladders¹² of atoms inside the lattice. In all those experiments the atoms were trapped in the lattice potential and occupied its allowed energy bands. In the suggested periodic mirror the potential is also a 1-D lattice, but the atoms strike the potential from the outside, and atoms with energies inside the forbidden energy gaps of the potential are reflected.

In the following we analyze reflection of atoms from both positive and negative potentials (blue- and red-detuned light, respectively), where the kinetic energy of the atoms is always above the potential height. The energies of the reflection bands and their width as a function of the potential height are calculated, and the relation between the reflection from the periodic potential to that from a single cell is derived. Next, the phase shift and the spontaneous-emission rate during the reflection are calculated. It is shown that atoms with kinetic energy of a few tens E_R above the potential, in a reflection bandwidth of $\sim 2E_R$, can be coherently reflected from a far-detuned periodic potential, created with available diode laser power. In the particular case of a red-detuned potential, Rb atoms with velocities of a few tens mm/s can be coherently reflected with probability close to one from a negative (attractive) potential.

2. REFLECTED ENERGY SPECTRUM

Consider a 1-D configuration, where two-level atoms move horizontally toward the light-induced potential and are then reflected from it. The potential is created with two monochromatic plane waves, which interfere and form a standing wave. The angle between the two waves, θ , can be different from π , so that along the x axis the potential extends over a limited range (see Fig. 1), and its period is $\Lambda = \lambda/[2 \sin(\theta/2)]$, where λ is the wavelength of the laser (for counterpropagating beams $\theta = \pi$ and $\Lambda = \lambda/2$). If the potential is created with far-detuned laser beams, several simplifying approximations for the atom-light interaction can be used. First, the dissipative force in the transverse direction [parallel to the z axis in Fig. 1(a)] can be neglected,¹³ and the only force caused by the light-atom interaction in that case is the dipole force. Second, if the laser detuning, δ , is large enough, such that $\delta \gg \gamma, \Omega_r$, then the dipole potential can be written as

$$U(x) = \hbar \Omega_r^2(x)/4\delta, \quad (1)$$

where γ is the natural linewidth and Ω_r is the Rabi frequency given by $\Omega_r^2(x) = (\gamma^2/2)[I(x)/I_s]$. Here $I(x)$ is the total light intensity in the point x and I_s is the saturation intensity. The above condition also ensures a low spontaneous-emission rate during the interaction, an essential condition for coherent reflection. A 1-D analysis is a good approximation if the atomic cloud is much smaller than the typical scale of changes of the potential in the transverse directions and if the gravitational fall of the atoms during the interaction is negligible.¹⁴

Consider now an atom with a kinetic energy E that is propagating along the x axis in the positive direction. Under the above assumptions, the spatial part of its wave function is a solution of the 1-D time-independent Schrödinger equation:

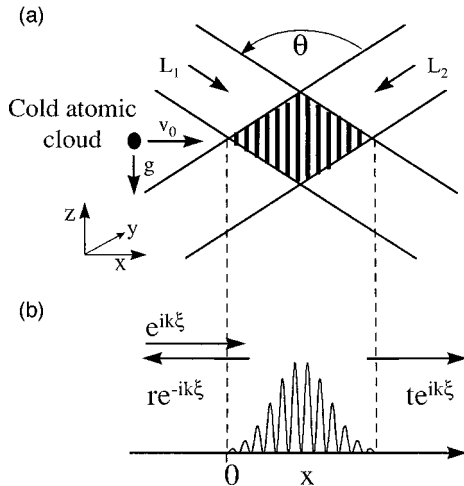


Fig. 1. Schematic diagram showing the two laser beams that interfere to form the periodic potential. (a) The orientation of the two laser beams ($L_{1,2}$) and the cold atomic cloud to be reflected. v_0 is the mean velocity of the atoms, and g indicates the gravitational acceleration. (b) The resulting 1-D potential, shown here with a Gaussian envelope. The propagation directions of the incident, reflected, and transmitted parts of the atomic wave function are also indicated.

$$-\frac{\hbar^2}{2m} \frac{d^2 \psi(x)}{dx^2} + U(x) \psi(x) = E \psi(x), \quad (2)$$

where the dipole potential is given by

$$U(x) = \frac{A(x)U_0}{2} [1 + \cos(2k_\Lambda x)]. \quad (3)$$

Here $k_\Lambda = \pi/\Lambda$, U_0 is the potential amplitude (peak to peak), which is derived from the laser parameters by Eq. (1), and $A(x)$ is a slowly varying envelope function that depends on the energy profile of the laser beams. We begin with the simple case of a rectangle envelope, $A(x) = 1$ for $0 < x < N\Lambda$, and $A(x) = 0$ elsewhere (N is the number of potential cells), and in the next section we analyze other envelope functions.

Equation (2) is transferred to dimensionless variables, by counting energy in units of the standing-wave equivalent recoil energy, $E_\Lambda = \hbar^2 k_\Lambda^2 / 2m$ (for $\theta = \pi$, $E_\Lambda = E_R$), and distance in units of the potential period Λ . Using the dimensionless variables $\epsilon = E/E_\Lambda$, $V = U/E_\Lambda$, and $\xi = k_\Lambda x$, Eqs. (2) and (3) become

$$-\frac{d^2 \psi}{d\xi^2} + \frac{A(\xi)V_0}{2} [1 + \cos(2\xi)] \psi = \epsilon \psi. \quad (4)$$

The solutions of Eq. (4) outside the potential are of the form

$$\begin{aligned} \psi(\xi) &= \exp(ik\xi) + r \exp(-ik\xi), & \text{for } \xi < 0, \\ \psi(\xi) &= t \exp(ik\xi), & \text{for } \xi > N\Lambda. \end{aligned} \quad (5)$$

Inside the potential, Eq. (4) is the well-known Mathieu equation,¹⁵ and its solutions have a more complex shape. However, it is possible to calculate the amplitude reflection and transmission coefficients, r and t , without calculating the wave function itself. For that purpose we used the method of transmission-line analogy.¹⁶ Briefly, the method is using an analogy between the 1-D Schrödinger equation and the equation for electrical-wave propagation in a transmission line. The transmission line is solely characterized by its impedance, and an analog wave impedance is introduced, so methods developed for transmission-line analysis can be used to numerically solve the 1-D Schrödinger equation with an arbitrary potential shape. The equivalent impedance of the potential is calculated backward, from right to left. First, the load impedance of the region with zero potential to the right is calculated, and then the impedance of the whole potential is calculated in recursive steps, until the beginning of the potential ($x = 0$) is reached. Finally, the reflection coefficient is derived from the difference between the impedance of the potential and that of the zero potential region to the left ($x < 0$). We found that computing time using that method was typically a hundred times shorter than using methods based on direct integration of Eq. (4). (In Section 4 we use the integration method to obtain the wave function itself).

The reflection coefficient, $R = |r|^2$, was calculated with the transmission-line method for different V and ϵ . A typical solution is given in Fig. 2, for a potential height $V_0 = \pm 40$, and N of 10, 100, and 1000 potential cells. Some general features of the reflected energy spectrum

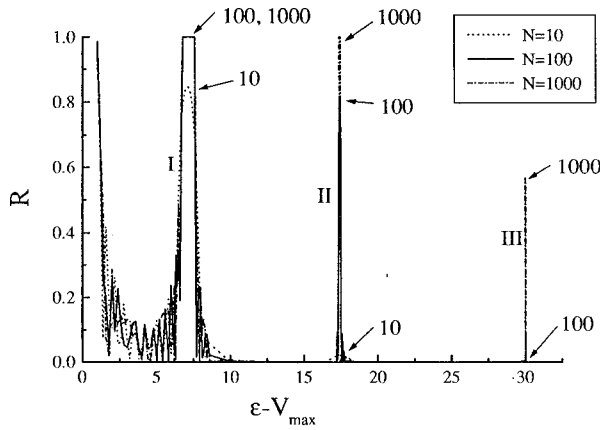


Fig. 2. Reflection coefficient from a periodic cosine potential with a rectangle envelope, for different numbers of potential cells, $N = 10$, $N = 100$, and $N = 1000$ in dashed, solid, and dash-dotted curves, respectively. The normalized potential amplitude is $V_0 = 40$, either blue or red detuned. The horizontal axis is the normalized atomic kinetic energy above the potential maximum, $\epsilon - V_{\max}$.

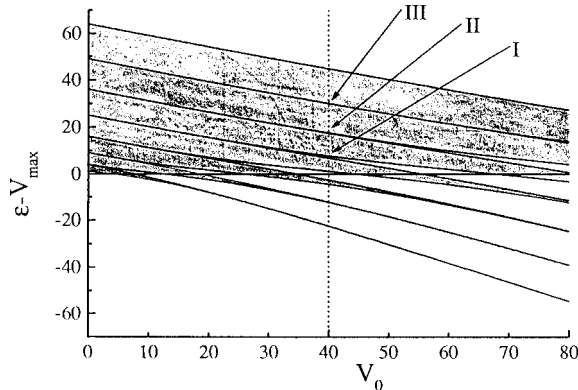


Fig. 3. Energy spectrum of the Mathieu equation. The vertical axis is the normalized energy of the atom above the potential maximum, and the horizontal axis is the normalized potential amplitude V_0 . The gray area indicates the allowed bands of the potential, and the white areas are the forbidden bands, in which reflection occurs. The arrows indicate the first three forbidden energy gaps of the $V_0 = 40$ potential.

clearly emerge. First, the reflection bands for the blue and red detunings are in the same energies above the potential maximum, i.e., $R_{\text{blue}}(\epsilon - V_{\max}) = R_{\text{red}}(\epsilon - V_{\max})$, where V_{\max} is the maximum of the potential. For a positive (negative) potential, $V_{\max} = V_0$ ($V_{\max} = 0$). Second, the higher the energy of the reflection band above the potential, the more cells are needed to achieve a given value of reflection, and the reflection band gets narrower. That dependence can be understood in terms of the reflection from a single potential cell, which is discussed in the next section.

An interesting situation occurs when the potential is very weak, since substantial reflection may occur even for atoms with energies much larger than the potential for values of N that are readily achieved experimentally. For example, a potential as low as $1/1000 E_R$, 3000 cells long (~ 1 mm), will reflect atoms with energy of $1E_R$, with $R \approx 0.6$. The reflection bandwidth in that case is very small, $\sim 3 \times 10^{-4} E_R$. In that case, it is clear that

the reflection is actually a first-order Bragg reflection of the atom from the periodic potential. It can also be interpreted as absorption of a photon from one of the light beams by the atom, followed by stimulated emission of a photon to the other beam, with a total change of $2\hbar k_\Lambda$ in the momentum of the atom along the x direction.

For a very large number of potential cells the problem of calculating the reflected energy bands is analogous to the problem of calculating the forbidden energy bands of a particle with energy $E > U_0$, which is found in the potential $U(x)$ with periodic boundary conditions. These bands for a potential of the form $U(x) = (U_0/2)[1 + \cos(2k_L x)]$ were discussed in the context of optical lattices,¹⁷ and are readily calculated with methods used in solid state physics.¹⁸ The energy bands for that potential, as a function of the potential height, are given in Fig. 3, as they serve a useful tool in the following discussion of the reflection. It can be seen that the forbidden bands are at the same energies as the reflected energies of Fig. 2.

The values of the reflected energies do not have a simple analytic dependence on the potential height. However, approximated values for the center of the reflectance bands can be found from the following arguments, which give physical insight to the reflection process. Let $k_0 = \sqrt{\epsilon}$ and $k(\xi) = [\epsilon - V(\xi)]^{1/2}$ be the atom's normalized wave number outside and inside the potential, respectively. The phase delay of a matter wave reflected after one potential cell (and thus going twice through the cell) with respect to the phase of a wave reflected from the previous cell is

$$\phi_1 = 2 \int_0^\pi k(\xi) d\xi, \quad (6)$$

where the normalized length scale is used. This phase delay should equal $2\pi n$ (n an integer) for a constructive interference to occur. Expanding $k(\xi)$ to second order in powers of V/ϵ , the reflected energies are found to be

$$\epsilon_{\text{reflect}} \approx n^2 + \frac{V_0}{2} + \frac{V_0^2}{32n^2}. \quad (7)$$

Approximation (7) is almost identical to an approximation based on series expansion of the Mathieu functions,¹⁵ with the difference between them smaller than 0.5% over the whole range of parameters discussed hereinafter. However, it yields a clearer physical insight in the context of atom reflection.

3. REFLECTION FROM ONE POTENTIAL CELL AND THE REFLECTION BANDWIDTH

In this section the width of the reflection bands is analyzed and its connection to the reflection coefficient from one potential cell, r_1 , is derived. We also demonstrate how the reflection width can be controlled by changing the parameters of the standing wave, such as its amplitude and its period.

Let N_0 be the number of cells needed to achieve reflection of the order of 1. As seen in Figs. 2 and 3, the reflection bandwidth $\Delta\epsilon$ decreases, and N_0 increases when the mean energy of the band increases. N_0 depends on

the reflection from one cell, r_1 , in a simple and intuitive way. Since in the center of the band a constructive interference of the reflection amplitudes from all the potential cells occurs, the number of cells that are needed for a reflection amplitude of ~ 1 is expected to scale as $N_0 \approx |r_1|^{-1}$, which is confirmed in our numerical calculations.

Figure 4 shows the reflection coefficient $R_1 = |r_1|^2$ calculated for a single cosine potential cell with $V_0 = \pm 40$, as a function of the atom's normalized energy. For a one-cell cosine potential, the reflection coefficient for $\epsilon \gg V_0$ can be evaluated analytically by the Born approximation, as

$$R_1(\epsilon) \cong \frac{V_0^2 k_\Lambda^4 \sin^2[\Lambda \sqrt{(\epsilon - \langle V \rangle)}]}{16\epsilon^2 (\epsilon - k_\Lambda^2)^2}, \quad (8)$$

where $\langle V \rangle$ is the average of V .¹⁹ That approximation is also plotted in the figure, and the good agreement to the exact solution for high values of ϵ is apparent. The asymptotic behavior for large energies is found from approximation (8) to be $R \propto \epsilon^{-4}$. As seen in Fig. 4, the values of R_1 for red and blue detunings are usually different. However, in the center of the reflection bands, $R_{1,\text{red}} = R_{1,\text{blue}}$; therefore all quantities evaluated using R_1 (such as N_0 and the reflection bandwidth) are the same for both red- and blue-detuned potentials.

To find the dependence of the reflection bandwidth on the number of cells N_0 and hence on r_1 , consider again the model used in the previous section to approximate the reflected energies. In the center of the reflection band, reflections from all cells are in the same phase (up to $2\pi n$). However, a change in the energy of the atoms will change the phase of the reflection. The total reflection will fall to about half of its maximum value when the phase difference between the first and last cells, $\Delta\phi_N$, will change considerably from its value in the center of the band, say, by $\pi/2$ rad. $\Delta\phi_N$ is approximated by

$$\begin{aligned} \Delta\phi_N(\epsilon_0 + \Delta\epsilon) &= N\phi_1(\epsilon_0 + \Delta\epsilon) \\ &\approx N\phi_1(\epsilon_0) + N \left. \frac{d\phi_1}{d\epsilon} \right|_{\epsilon=\epsilon_0} \Delta\epsilon, \end{aligned} \quad (9)$$

where ϕ_1 is given by Eq. (6). Evaluating $d\phi_1/d\epsilon$ to a first order in (V/ϵ) , taking into account that $N\phi_1(\epsilon_0) = 2n\pi$, and equating the phase difference $\Delta\phi_N$ to $(2n + 1/2)\pi$ yields an estimate of the full width at half-maximum (FWHM) of the energy band, as

$$\Delta\epsilon \approx \frac{4\epsilon_0^{3/2}}{N_0(4\epsilon_0 + V_0)}. \quad (10)$$

N_0 was used in the last expression instead of N , since in a long potential the cells after N_0 have a very small contribution to the reflection. The reflection bandwidth for the first five bands of the $V_0 = 40$ potential are shown in Fig. 5, both from a direct solution of the Mathieu equation and from approximation (10). The fast decrease in $\Delta\epsilon$ with increasing ϵ , as well as the agreement between the two methods of evaluation, is evident.

Reflection bandwidths much narrower than $1E_R$ are not easy to measure in an experiment owing to the high velocity resolution needed and the low number of re-

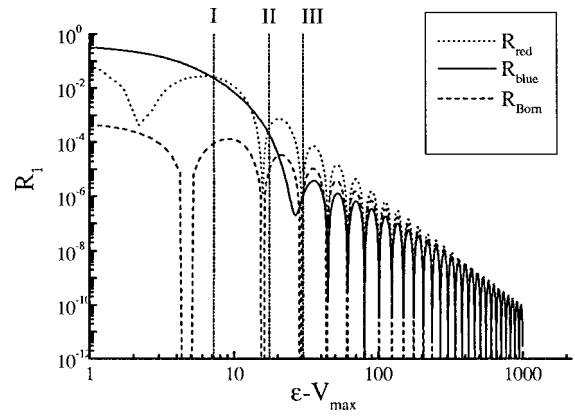


Fig. 4. Reflection coefficient from a single $V_0 = 40$ cosine potential cell versus the normalized kinetic energy above the potential maximum, for red (dotted curve) and blue (solid curve) detuning of the laser. The Born approximation of Eq. (8) is given as a dashed curve. The energies of the first three reflection bands of the periodic potential are also marked.

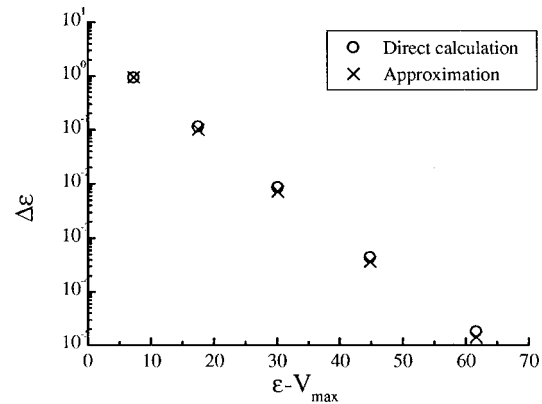


Fig. 5. Width of the first five reflection bands of the $V_0 = 40$ potential as a function of the band mean energy. Both energy mean and bandwidth are shown in normalized units. The values obtained from a numerical calculation of the energy bands of the Mathieu equation are marked with 'O', and the values obtained from approximation (10) are marked with 'X'.

flected atoms. We describe here two methods in which the reflection bands can be largely broadened: the first achieves broader bandwidth using a nonuniform envelope of the potential, the second by changing its period gradually (chirp). The first method may be intuitively understood with the aid of Fig. 3, considering the nonuniform potential to be composed of several adjacent uniform regions. Each region will act as a periodic mirror having a different potential and thus different reflected energies. If the slope of the potential envelope is properly adjusted, these different reflection bands can just overlay so as to form a much wider and continuous band (for the price of a longer potential). In an experiment it is most convenient to use a Gaussian potential envelope, by use of readily available Gaussian laser beams.

In Fig. 6 the calculated second reflection band of a potential with a truncated half-Gaussian envelope²⁰ is shown, in a solid curve. The potential length is 700 cells. As can be seen, the reflection bandwidth is $\sim 2E_R$, ~ 10 times higher than for the constant envelope case. The reflection coefficient is not constant over the reflection

band since R_1 is different for different potential heights, and thus the number of cells needed for a given reflection changes. Similar results were obtained for other smooth potential envelopes, such as a linearly varying one. The envelope of the potential can be tailored so as to yield a constant reflection coefficient over the entire band.

The second method to increase the reflection bandwidth involves nonuniform period of the potential. The second reflection band from a chirped potential is also shown in Fig. 6, in a dashed curve. The period changes linearly from $2.01k_\Lambda$ to $1.985k_\Lambda$ along the potential (1.25% change in the period). Here, also, the bandwidth increased to $\sim 2E_R$, and the number of cells is 700. Such a potential can be achieved, for example, if the standing wave is made of one collimated wave (with linear phase fronts) and one wave with spherical wave fronts (for 1-mm-diameter beams, a 1% chirp requires a 100-mm radius of curvature of the wave fronts²¹). In both methods, similar results were achieved. The number of cells needed for a substantial reflection increases in proportion to the increase in the bandwidth, consistent with the intuitive concept of an incoherent superposition of reflections from different regions of the potential.

Next, we give a specific example for reflection of Rb atoms from a mirror that can be formed with practical laser parameters. For linearly polarized light and δ much larger than the excited-state hyperfine splitting of the atom, the optical dipole potential is uniform among the magnetic sublevels, and the two-level model may be used. The potential height of $U_0 = 40E_\Lambda$, which was discussed above, can be produced, for example, with a 500-mW laser, split into two beams of 2.2-mm diameter that intersect each other at an angle of $\theta = 120^\circ$, and a detuning of 100 GHz (0.2 nm) with respect to the ^{85}Rb D_2 line. Table 1 summarizes the reflection parameters for the lowest three reflection bands. The reflected energies above the potential are those of Fig. 2, and R_1 is taken from Fig. 4. The number of cells needed to get a reflection of the order of one is given together with the physical length of the potential, which is lower than the beam's diameter in all three bands. However, $\Delta\epsilon$, calculated from approximation (10), is very low for the third band, hence an additional length noted as $L_{\Delta\epsilon\approx 1}$ is presented, which is the length needed for a reflection bandwidth of $\sim 1E_\Lambda$ by a chirped potential. With the above parameters a bandwidth of $1E_\Lambda$ cannot be achieved in the third band, since $L_{\Delta\epsilon\approx 1}$ is longer than the diameter of the beams. The specific example is further discussed in the next section.

4. COHERENCE, PHASE DELAYS, AND INTERACTION TIMES

Several important characteristics of the periodic mirror are analyzed in this section: the interaction time of the atom with the light field, the probability for spontaneous emission during the reflection, and the phase acquired by the reflected atoms. Evaluation of the interaction time allows the gravitational fall during the interaction to be determined, in order to confirm the validity of the 1-D model for the periodic mirror. A low spontaneous-emission rate is essential for the coherence of the reflection and for the transverse scattering force to be negli-

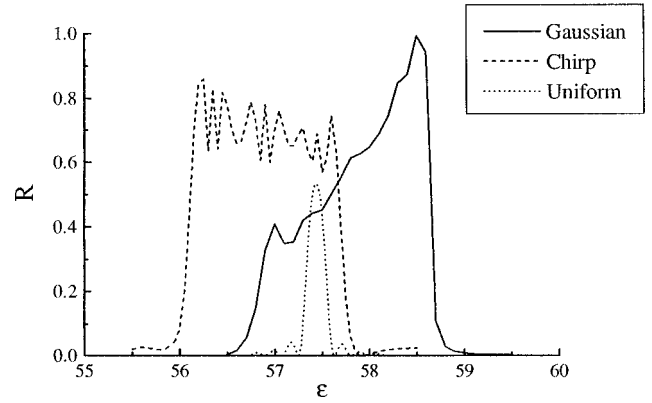


Fig. 6. Second reflection band from a potential with a truncated half-Gaussian envelope (see text), solid curve, and from a chirped potential, dashed curve. Parameters of the half-Gaussian are $\sigma = 1770\Lambda$ and $V_0 = 42$ (maximal potential height). Parameters for the chirped potential: period changes linearly from 2.01ξ to 1.985ξ and $V_0 = 40$. The number of cells in both cases is $N = 700$. The reflection from a uniform envelope and period potential with $N = N_0 = 63$ is also shown (dotted curve) as a reference.

Table 1. Numerical Values of the Reflection Parameters for the First Three Reflection Bands from a $V_0 = 40$ Potential

Reflection Parameters	Reflection Band		
	I	II	III
$\langle \epsilon \rangle - V_{\max}$	7.2	17.46	30.036
$R_1 = r_1 ^2$	2.8×10^{-2}	2.5×10^{-4}	1×10^{-6}
$N_0 = r_1^{-1}$	6	63	1000
$L = N_0\Lambda$ (μm)	2.7	28	450
$\Delta\epsilon$	0.94	0.1	0.007
$L_{\Delta\epsilon\approx 1} = N_0\Lambda/\Delta\epsilon$ (μm)	3	285	64000

gible. The phase of the reflected atoms is a critical property for configurations for which coherence is important, such as atomic cavities, traps, and interferometers.

The interaction time of a particle with the potential can be calculated from the phase of the reflection coefficient. The time delay, in normalized units, is measured in units of ω_Λ^{-1} (where $\omega_\Lambda = E_\Lambda/\hbar$ is the standing-wave equivalent recoil frequency) and is given by²²

$$\tau = \left(\frac{d\phi}{d\epsilon} \right)_{\epsilon=\epsilon_0}, \quad (11)$$

where ϕ is the phase of the reflection coefficient [r in Eq. (5)], and the derivative is evaluated at the kinetic energy of the incoming atom. We calculated $\phi(\epsilon)$ with the method of transmission line described above, and we calculated the time delay using Eq. (11). The results for the $V_0 = 40$ potential are given in Fig. 7. In Fig. 7(a) the phase inside the first and second reflection bands above the potential is shown. The results are the same for both positive and negative potentials (keeping in mind that the x axis is $\epsilon - V_{\max}$). In Fig. 7(b) the time delay is given, both in normalized units and in seconds, where data for ^{85}Rb were used. It can be seen that the time delay in the second band is almost an order of magnitude larger than

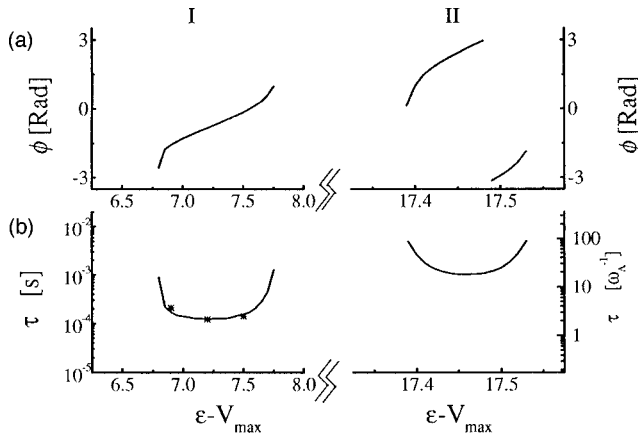


Fig. 7. (a) Relative phase of the reflection from a $V_0 = 40$ potential, in the first and second reflection bands. (b) Interaction time of the atom with the potential in the same energy bands. Time values are given both in normalized units and in seconds, for ^{85}Rb atoms and parameters as in text. The solid curve is calculated from the phase of the reflection, with Eq. (11), and the asterisks are values calculated from the wave function by use of Eq. (13). Note the different scale of the energy axis in the two bands.

in the first band, which is consistent with its N_0 , which is 63 compared to 6 for the first (see Table 1).

The time delay in the case of a total reflection can be calculated also from the wave function inside the potential. Consider an atom that is moving from a very far point $-X$ toward the potential and is then reflected from it and moves until it reaches $-X$ again. The velocity of the atom outside the potential is v_0 , and the total time for the movement is given by $T_{\text{tot}} = 2X/v_0 + \tau \equiv T + \tau$. The ratio τ/T can be interpreted as the probability to find the atom inside the potential during one reflection, when $X \rightarrow \infty$. On the other hand, the same probability is given by the normalized square of the wave function inside the potential:

$$\frac{\int_0^\infty |\psi(x)|^2 dx}{\int_{-X}^\infty |\psi(x)|^2 dx} = \frac{\int_0^\infty |\psi(x)|^2 dx}{\int_{-X}^0 |\psi(x)|^2 dx + \int_0^\infty |\psi(x)|^2 dx} \xrightarrow{X \rightarrow \infty} \frac{\int_0^\infty |\psi(x)|^2 dx}{X/2}. \quad (12)$$

Here the wave function ψ is normalized such that its amplitude equals one to the left of the potential.²³ Equating the two results for the probability of finding the atom inside the potential, we find the interaction time in units of ω_Λ^{-1} , as

$$\tau = \frac{2 \int_0^\infty |\psi(\xi)|^2 d\xi}{k_0}, \quad (13)$$

where $k_0 = \sqrt{\epsilon}$ is the normalized velocity of the incoming atom.

To evaluate τ in that method, the wave function was calculated with a direct numerical integration of Eq. (4).

A transmitted wave of the form $\exp(ik\xi)$ is assumed as the solution to the right of the potential ($\xi > N\Lambda$), and the equation is solved in the reverse direction, from right to left. The resulting wave function is then normalized as discussed above. The interaction time was calculated in that method for three energies inside the first band and is shown as asterisks in Fig. 7(b). The good agreement between the two calculation methods is apparent.

In a similar way, the average number of spontaneously scattered photons during the reflection can be calculated. An atom found inside the potential, in a given light intensity and detuning, scatters photons at the rate

$$\gamma_s(\xi) = \frac{\gamma^3}{8\delta^2} \times \frac{I(\xi)}{I_s} = \frac{\gamma\omega_\Lambda V(\xi)}{\delta}. \quad (14)$$

Now, to determine S , the number of spontaneously scattered photons during a reflection, that rate has to be normalized by the probability distribution of the atom inside the potential, as

$$S = \frac{2 \int_0^\infty |\psi(\xi)|^2 \gamma_s(\xi) d\xi}{k_0 \omega_\Lambda}. \quad (15)$$

The reflection may be regarded as coherent when $S \ll 1$. From Eqs. (13) and (15) it is evident that the longer the interaction time, the higher is the spontaneous-emission rate. From that reason the reflection at higher energy bands, which requires longer potential for reflection and hence longer interaction times, has also a higher spontaneous-emission rate. For very long potentials the numerical accuracy of the integration of the wave function is limited; hence for high reflection bands (large N_0), S was approximated by the average of the potential in Eqs. (14) and (15). The accuracy of that approximation was found to be about a factor of 2 compared with the exact result.

In order to use the periodic potential as a mirror or a beam splitter in atomic interferometers, it is important to know the total phase of the reflected and transmitted atoms, and its sensitivity to experimental parameters. A common method for the calculation of the total phase is by integrating the ac Stark shift over the classical trajectory of the atom.² In the case of the periodic potential, however, that approximation cannot be used owing to the short length scale of changes in the potential compared with the atomic wave-packet uncertainty. Therefore it is possible to calculate only the sensitivity of the reflection phase to the experimental parameters. As an example, we calculated the phase change for the second reflection band of the $V_0 = 40$ potential to be $\Delta\phi = 400\Delta I/I$ with respect to the laser intensity. Such dependence requires laser intensity stability better than $\sim 1:400$ to prevent reduction in the fringe contrast of atomic interferometers and much better stability to prevent systematic shifts in the measured quantities.

Coming back to the numerical example of the previous section, the interaction time and the number of spontaneously scattered photons during the reflection are given in Table 2. The velocity of the reflected atoms outside the potential and the gravitational fall during the interaction are also given. The gravitational fall in all bands is

Table 2. Numerical Values of the Velocities, Interaction Time, Gravitational Fall, and Spontaneous-Scattering Rates, for the First Three Reflection Bands of a $V_0 = 40$ Periodic Potential^a

Parameters	Reflection Band		
	I	II	III
v_{red} (mm/s)	13.9	21.7	28.5
v_{blue} (mm/s)	35.7	39.4	43.5
τ (ms)	0.12	1.0	10.3
h , gravitational fall (μm)	0.07	5	530
S_{red}	0.0020	0.028 ^b	0.291 ^b

^aValues are for ⁸⁵Rb atoms, and the laser parameters are $I = 6500 \text{ mW/cm}^2$ in each beam, $\theta = 120^\circ$, and $\delta = \pm 100 \text{ GHz}$ for blue/red detuning.

^bApproximation, accuracy limited to a factor of 2 due to the long potential (see text).

lower than the diameter of the beams. However, if the potential would be modified to enlarge the bandwidth of the reflection to $\sim 1E_\Lambda$, the interaction time would increase, and hence the gravitational fall for the third band would extend out of the potential. Moreover, in that case the spontaneous-scattering rate for that band would be larger than one photon per reflection, which destroys the coherence of the reflection. In contrast to the case of a far-detuned light trap,²⁴ here the spontaneous-emission rate for a red-detuned laser is lower (by a factor of ~ 0.6) than for a blue-detuned one. The reason is that the wave function is concentrated near the potential peaks, which have high light intensity for blue detuning but are dark for a red-detuned laser. We conclude that for an atomic cloud with diameter of $\sim 200 \mu\text{m}$ or smaller, the 1-D approximation is valid for the first and second bands, and so is the model that ignores the spontaneous emission. If the potential would be linearly chirped, with $\sim 1\%$ change in its period the reflection bandwidth in the second band will be $\sim 1E_R$ FWHM, and atoms with velocity of $39.4 \pm 0.4 \text{ mm/s}$ ($21.7 \pm 0.8 \text{ mm/s}$) will be quantum reflected from a blue (red) detuned potential.

5. CONCLUSIONS

We presented a theoretical analysis of the quantum reflection of cold atoms from a periodic light-induced dipole potential. The reflection occurs in discrete energy bands, which correspond to the forbidden energy gaps of an infinite potential. A simple model based on coherent interference of atomic wave functions along the potential was introduced. This model gives good approximations for the values of the centers of the reflected energy bands and their widths. The connection between the reflection bandwidth, the number of cells needed to get a substantial reflection, and the reflection coefficient from one potential cell was derived. It is interesting to note that the reflection from one rectangle potential cell is much higher than from a cosine potential cell, especially in high energies above the potential. As a result, a periodic rectangle potential has much wider reflection bands high above the potential, as compared with a cosine potential with the

same height, period, and number of cells. The last result can be generalized to conclude that, as each potential cell becomes steeper, the periodic potential will have wider reflection bands at higher energies.

Other properties of the periodic mirror, which are of importance for experimental realizations, were also treated. We have shown that the reflection bandwidth can be increased by using incoherent superposition of reflections from different parts along the potential, using nonuniform envelope or period. Expressions for the spontaneous-emission rate during the reflection and for the interaction time of the atom with the potential were derived, based on the time-independent atomic wave function. As expected, in higher reflection bands, for which longer potential is needed to achieve high reflection, the interaction time is larger and so is the spontaneous-emission rate. In a specific example, for ⁸⁵Rb atoms, we have shown that, for potential depth and detuning that can be achieved with available laser power, atoms with velocities of a few tens mm/s can be coherently reflected from both positive and negative periodic potential.

A periodic potential can serve also as a coherent atomic beam splitter, where its length can be tailored to give any desired reflection/transmission ratio. With the parameters of the above example, a momentum difference of more than $10\hbar k$ with angular separation of 180° between the two parts of the atomic wave packet can be achieved, which may be very useful for atomic interferometers. Unlike other suggested atomic beam splitters, which also have a momentum separation of a few tens $\hbar k$,^{25,26} this periodic potential beam splitter has only two narrow diffraction orders (reflection and transmission), and the large detuning enables the beam splitter to act on cold atoms coherently, with a negligible spontaneous-emission rate. Other possible applications of the periodic potential, in analogy to periodic structures in optics, may be narrow velocity filters and high-reflection narrow-bandwidth mirrors for atomic cavities.

ACKNOWLEDGMENTS

This work was supported in part by the Minerva Foundation and by the Israel Science Foundation.

REFERENCES AND NOTES

1. V. I. Balykin, V. S. Letokhov, Yu. B. Ovchinnikov, and A. I. Sidorov, "Quantum-state-selective mirror of atoms by laser light," *Phys. Rev. Lett.* **60**, 2137 (1988).
2. M. A. Kasevich, D. S. Weiss, and S. Chu, "Normal-incidence reflection of slow atoms from an optical evanescent wave," *Opt. Lett.* **15**, 607 (1990).
3. C. G. Aminoff, A. M. Steane, P. Bouyer, P. Desbiolles, J. Dalibard, and C. Cohen-Tannoudji, "Cesium atoms bouncing in a stable gravitational cavity," *Phys. Rev. Lett.* **71**, 3083 (1993).
4. C. Henkel, C. I. Westbrook, and A. Aspect, "Quantum reflection: atomic matter-wave optics in an exponential potential," *J. Opt. Soc. Am. B* **13**, 233 (1996).
5. P. Verkerk, B. Lounis, C. Salomon, C. Cohen-Tannoudji, J. Y. Courtois, and G. Grynberg, "Dynamics and spatial order of cold cesium atoms in a periodic optical potential," *Phys. Rev. Lett.* **68**, 3861 (1992).
6. P. S. Jessen, C. Gerz, P. D. Lett, W. D. Phillips, S. L.

- Rolston, R. J. C. Spreeuw, and C. I. Westbrook, "Observation of quantized motion of Rb atoms in an optical field," *Phys. Rev. Lett.* **69**, 49 (1992).
7. A. Hemmerich and T. W. Hansch, "2-dimensional atomic crystal bound by light," *Phys. Rev. Lett.* **70**, 410 (1993).
 8. G. Grynberg, B. Lounis, P. Verkerk, J. Y. Courtois, and C. Salomon, "Quantized motion of cold cesium atoms in 2-dimensional and 3-dimensional optical potentials," *Phys. Rev. Lett.* **70**, 2249 (1993).
 9. G. Birkl, M. Gatzke, I. H. Deutsch, S. L. Rolston, and W. D. Phillips, "Bragg scattering from atoms in optical lattices," *Phys. Rev. Lett.* **75**, 2823 (1995).
 10. M. Weidemuller, A. Hemmerich, A. Gorlitz, T. Esslinger, and T. W. Hansch, "Bragg diffraction in an atomic lattice bound by light," *Phys. Rev. Lett.* **75**, 4583 (1995).
 11. M. Ben Dahan, E. Peik, J. Reichel, Y. Castin, and C. Salomon, "Bloch oscillations of atoms in an optical potential," *Phys. Rev. Lett.* **76**, 4508 (1996).
 12. S. R. Wilkinson, C. F. Bharucha, K. W. Madison, Q. Niu, and M. G. Raizen, "Observation of atomic Wannier-Stark ladders in an accelerating optical potential," *Phys. Rev. Lett.* **76**, 4512 (1996).
 13. J. P. Gordon and A. Ashkin, "Motion of atoms in a radiation trap," *Phys. Rev. A* **21**, 1606 (1980).
 14. The mirror can also be formed in the z direction, such that the atoms move vertically, in a trampoline configuration. However, in this case the gravitation potential must be included in the analysis, which is not treated here.
 15. N. W. McLachlan, *Theory and Application of Mathieu Functions* (Oxford University, London, 1947), Chap. 2.
 16. A. N. Khondker, M. Rezwani Khan, and A. F. M. Anwar, "Transmission line analogy of resonance tunneling phenomena: the generalized impedance concept," *J. Appl. Phys.* **63**, 5191 (1988).
 17. L. S. Letokhov and V. G. Minogin, "Trapping and storage of atoms in a laser field," *Appl. Phys.* **17**, 99 (1978).
 18. N. W. Ashcroft and N. D. Mermin, *Solid State Physics* (Holt, Rinehart & Winston, New York, 1976), Chap. 9.
 19. $[(\epsilon - \langle V \rangle)]^{1/2}$ was used in the argument of the sine (instead of $\sqrt{\epsilon}$), which leads to a better accuracy in the phase.
 20. A truncated half-Gaussian envelope of the shape $\exp(-\xi^2/2\sigma^2)$ for $0 \leq \xi \leq N\Lambda$, and 0 elsewhere, was used. For a full-Gaussian envelope the reflected amplitudes from regions of equal height in both sides of the potential interfere, which adds narrow fringes to the reflected energy spectrum.
 21. Note that for spherical wave fronts the interference fringes are not perfectly parallel. With the parameters given in the text, the angle of the fringes will change by $\pm 3^\circ$ over a 1-mm interaction range, which might call for a two-dimensional treatment, depending on the size of the atomic cloud.
 22. C. Cohen-Tannoudji, B. Diu, and F. Laloe, *Quantum Mechanics*, 2nd ed. (Wiley, New York, 1977), Vol. 1, Chap. 1.
 23. In the case of total reflection the reflection coefficient can be written as $r = \exp(i\phi)$, and the probability distribution to the left of the potential is then $|\psi(\xi)|^2 = a \cos^2(k\xi - \phi/2)$. The normalization used is $a = 1$.
 24. N. Davidson, H. J. Lee, C. S. Adams, M. Kasevich, and S. Chu, "Long atomic coherence times in an optical dipole trap," *Phys. Rev. Lett.* **74**, 1311 (1995).
 25. T. Pfau, Ch. Kurtsiefer, C. S. Adams, M. Sigel, and J. Mlynek, "Magneto-optical beam splitter for atoms," *Phys. Rev. Lett.* **71**, 3427 (1993).
 26. K. S. Johnson, A. Chu, T. W. Lynn, K. K. Berggren, M. S. Shahriar, and M. Prentiss, "Demonstration of a nonmagnetic blazed-grating atomic beam splitter," *Opt. Lett.* **20**, 1310 (1995).